On the differences of transitional separated-reattached flows over leading-edge obstacles of varying geometries

I. E. Abdalla
Faculty of Technology, Department of Engineering, DeMontfort University, Leicester, UK

Abstract

Large-eddy simulation (LES) of transitional separating-reattaching flow on three different geometries including a square surface mounted obstacle (referred to hereafter as the *obstacle*), a forward facing step (FFS) and square leading edge plate aligned horizontally to a flow field, has been performed using a dynamic sub-grid scale model. The Reynolds number based on the uniform inlet velocity and the plate thickness, obstacle/step height varies in the range of $4.5 - 6.5 \times 10^3$. The mean LES results for three geometries compare reasonably well with the available experimental and DNS data.

As the obstacle and FFS are characterised by an additional separated region upstream the separation line compared to the square leading edge plate, this is thought to have led to some differences observed both on the flow topology and turbulence spectrum downstream the leading edge for the three geometries. The spectra obtained using standard Fourier transform for positions downstream the leading edge plate has clearly captured the characteristic shedding frequency but not in the case of the obstacle and FFS. However, the spectra content at locations within the upstream separated region for the obstacle and FFS indicates that the upstream bubble is unstable via the Kelvin-Helmholtz (K-H) mechanism which might have an influence on both the spectra content, instability mechanism and the flow topology of the downstream separated region.
Keywords: large-eddy simulation, transition to turbulence, coherent structures, shedding.

WIT Transactions on Modelling and Simulation, Vol 48, © 2009 WIT Press
www.witpress.com, ISSN 1743-355X (on-line)
doi:10.2495/CMEM090301

1 Introduction

The physics of transitional and turbulent separated-reattached flows generated by leading-edge obstacles has relevance to many applications in engineering and environment. Calculation of wind loads on structures, the spread of pollutants in the vicinity of buildings, turbo-machinery industry and aerodynamics of road vehicles and aircraft are few applications to mention.

Of interest in this paper is the transitional separated-reattached flows created by means of a sharp leading-edge geometries including a square leading edge plate aligned horizontally to a flow field, an obstacle and a FFS. The flow over a surface-mounted bluff bodies is complex when compared with other leading body geometries such as the backward-facing step and the square leading edge plate case. The complication comes as a result of an additional separation in the upstream region caused by the obstruction flow leading to the question of whether the upstream separated region behaves as a closed or open bubble and what influence does such separation bubble has on the downstream separated-reattached flow. This study compare some few fundamental features associated with separated-reattached flows for the three geometries mentioned above.

2 Details of numerical computation

The filtered Navier-Stokes equation are discretised on a staggered grid using the finite volume method. Smaller-scale motion that are smaller than the control volume are averaged out and are accounted for by a subgrid-scale model. A standard dynamic subgrid model in Cartesian co-ordinate has been employed in the present study. The explicit Adams-Bashforth scheme is used for the momentum advancement. The Poisson equation for pressure is solved using an efficient hybrid Fourier multigrid method. The spatial discretisation is second order-order central differencing which is widely used in LES owing to its non-dissipative and conservative properties. More details of the mathematical formulation and numerical methods have the reader elsewhere by Yang and Voke [1] and Abdalla *et al.* [2]

3 Flow configuration, mesh and boundary conditions

For the three simulations, a free-slip but impermeable boundary is applied at the lateral boundary. In the spanwise direction, the flow is assumed to be statistically homogeneous and periodic boundary conditions are used. No-slip boundary conditions are used at all other walls. At the inflow boundary, a uniform velocity profile is applied. At the outflow boundary, a convective boundary condition is applied. The two-dimensionality of the flow was broken by means of a random perturbation (20% of the inflow velocity) applied for a limited number of time steps (exactly 250 time steps for the three simulations) at the very early stages of the simulation.

For the obstacle case, the grid consists of $288 \times 128 \times 64$ cells along the streamwise, wall-normal and spanwise directions respectively with dimensions of the

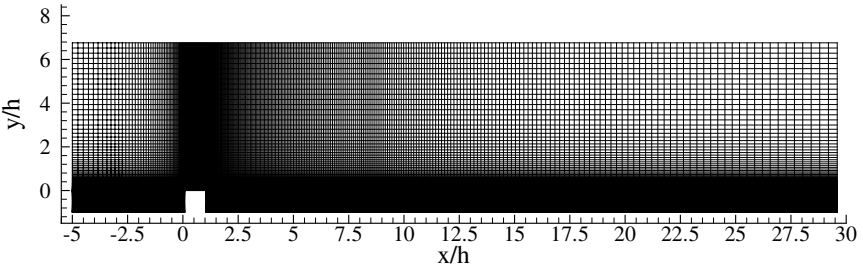

Figure 1: The computational domain and mesh used for the obstacle geometry.

domain as $35h * 8h * 4h$ (h is the obstacle height). In terms of wall units based on the friction velocity downstream of reattachment at $x/h = 27$, the streamwise mesh sizes vary from $\Delta x^+ = 6.77$ to $\Delta x^+ = 43.04$, while $\Delta z^+ = 10.625$ and at the wall $\Delta y^+ = 1.28$. The time step used in this simulation is 4.75×10^{-6} second ($0.001425\frac{h}{U_0}$). The simulation ran for 129,000 time steps equivalent to more than 5 flow passes through the domain (or residence times) to allow the transition and turbulent boundary layer to be established, i.e. the flow to have reached a statistically stationary state. The averaged results were gathered over a further 249,900 steps, with a sample taken every 10 time steps (24,990 samples) averaged over the spanwise direction too, corresponding to more than 10 flow passes or residence times. The computational domain and mesh used for the obstacle case is shown in Figure 1 as an illustration of how the grid is stretched for proper resolution of the flow features.

For the FFS, the grid consists of $320 \times 220 \times 64$ cells along the streamwise, wall-normal and spanwise directions respectively with dimensions of the domain as $25h * 8h * 4h$ (h is the step height). The time step used in this simulation is 1.5×10^{-6} s ($0.010125\frac{h}{U_0}$). The FFS case ran for a total of 404,000 time step with the sampling for the mean field started 100,000 after the start of the run. In terms of wall units based on the friction velocity downstream of reattachment at $x/h = 23$, the streamwise, wall normal and spanwise mesh sizes are $\Delta x^+ = 19.98$, while $\Delta z^+ = 10.94$ and at the wall $\Delta y^+ = 1.135$.

For the blunt leading-edge flat plate, the grid consists of $256 \times 212 \times 64$ cells along the streamwise, wall-normal and spanwise directions respectively with dimensions of the domain as 25D*16D*4D where D is the plate thickness. In terms of wall units based on the friction velocity downstream of reattachment at $x/x_R = 2.5$ (x_R is the mean reattachment length) the streamwise mesh sizes vary from $x+ = 9.7$ to $x+ = 48.5$, $z+ = 20.2$ and at the wall $y+ = 2.1$. The time step used in this simulation is $0.001885D/U_0$. The simulation ran for $70,000$ time steps to allow the transition and turbulent boundary layer to become established. The averaged results presented below were then gathered over further 399,000 steps with a sample taken every 10 time steps (39,900 samples) averaged over the spanwise direction too, corresponding to around 28 flow-through or residence times.

4 Results and discussion

The time-mean length of the separation region is an important parameter characterising a separated/reattached flows. The method used here to determine the mean reattachment location is described in Hung *et al.* and involves determining the location at which the mean velocity $\bar{U} = 0$ at the first grid point away from the wall.

As an example, Figure 2 shows that the predicted a mean reattachment length downstream the leading edge for the obstacle is $\approx 15.5h$. Bergeles and Athanassiadis [3] reported a value of $x_R/h = 11$ for a turbulent boundary layer of thickness $0.48h$. Durst and Rastogi [4] reported a value of $x_R/h = 16$ also under a turbulent boundary layer condition. Similar scatter was reported for the fence geometry. Tropea and Gackstatter [5] reported a value of $x_R/h = 17$ under transitional flow conditions and the DNS study of Orellano and Wengle [6] reported $x_R/h = 13.2$ (12.8 for the LES with Smagorinsky model). Larsen [7] reported a value of $x_R/h = 11.7$ from his experimental work which was conducted for a large turbulence intensity. Comparing the current LES results with the results above, it is clear that the LES prediction is within the range for the current transitional flow.

The predicted mean reattachment length downstream of the step is 8.1 h. Ko [8] simulation predicted this length as 5.5 h and the measured value from the Moss and Baker [9] experiment is 4.8 h. In contrast with the current simulation it appears that the LES has over predicted this parameter. But once again the difference is thought to be due to the high Reynolds number and the nature of turbulent flows in the work cited here. However, the FFS step flow bear many similarities for the square leading edge geometry for which the predicted mean reattachment length is 6.5D. Castro and Epik [10] reported a value of 7.7D for a separated-reattached flow generated by a square leading edge flat plate at $Re_D = 6500$ which is comparable to the FFS and the square leading edge plate.

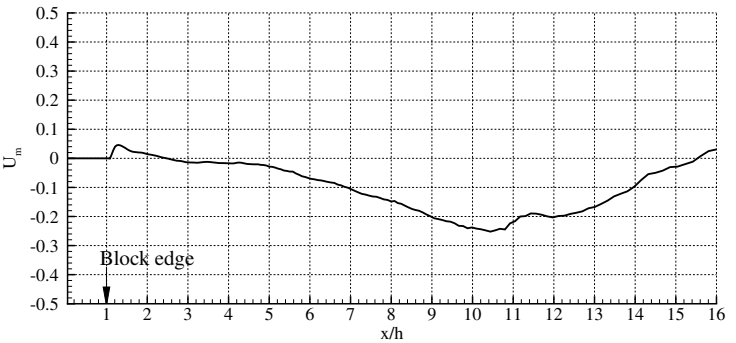

Figure 2: Profile of velocity $\bar{U} = 0$ at the first grid point away from the wall.

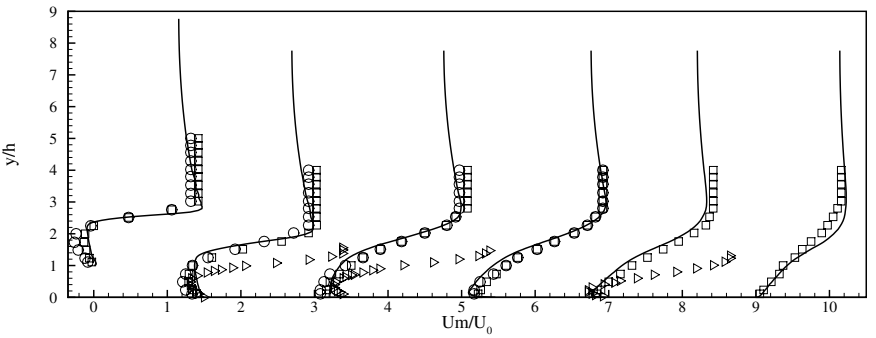

Figure 3: Obstacle flow: profiles of mean streamwise velocity U_m/U_0 at six streamwise locations measured from the separation line (leading edge). Left to right $x/x_R = 0.05, 0.2, 0.4, 0.6, 0.8, 1.025$. Also shown are measurements by Tropea and Gackstatter [5] (triangle), Larsen [7] (square) and the DNS data of Orellano and Wengle [6] (circle) at $\mathrm{Re} = 3{,}000$.

4.1 Mean and rms velocities

The current LES results for the obstacle and FFS are compared with relevant experimental and DNS data obtained from similar previous studies. Figure 3 compares the mean streamwise velocity distribution $\overline{U}/U_0$ at 6 locations downstream of the obstacle leading edge with the experimental data of Tropea and Gackstatter [5] (available only at 3 locations), Larsen [7] and the DNS data of Orellano and Wengle [6]. The results show good agreement with the data of Larsen [7] and the DNS data of Orellano and Wengle [6]. The free-stream velocities of the data from Tropea and Gackstatter [5] are bigger than those predicted by the LES and the other two results, and peak at lower y-values. One of the reasons for this difference is the could be attributed to the difference in blockage ratio used by Tropea and Gackstatter [5] which is very low (2, 5 in the case of Orellano and Wengle [6] and 8 for the current LES).

Profiles of the rms streamwise velocity, u_{rms}, normalised by U_0, at the same six stations are shown in Figure 4. The agreement between the LES results and the data of Larsen [7] and the DNS data of Orellano and Wengle [6] is encouraging. No measured data were presented by Tropea and Gackstatter [5]. It is worth to mention that data from the FFS and the square leading edge plate (not shown here) show a similar agreement with comparable experimental and computational data.

4.2 Differences in the flow field for the three cases

As mentioned above, the main difference between the obstacle and FFS from one side and the square leading edge plate from the other side is the upstream separated region present in the first two and it is absence in the later. Therefore, the main question that is raised here is: what will be the influence of the separated

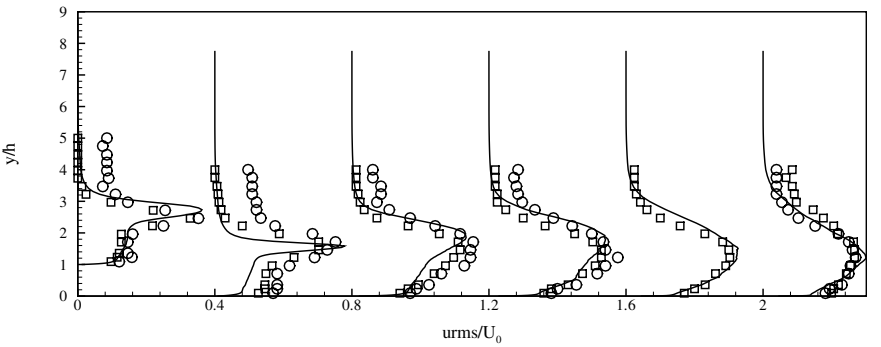

Figure 4: Obstacle flow: profiles of mean streamwise turbulent intensity u_{rms}/U_0 at six streamwise locations measured from the separation line (leading edge). Left to right $x/x_R = 0.05$, 0.2, 0.4, 0.6, 0.8, 1.025. Also shown are measurements by Larsen [7] (square) and the DNS data of Orellano and Wengle [6] (circle) at $\mathrm{Re} = 3{,}000$.

region upstream the obstacle and FFS flow on the bubble formed downstream the leading edge for the two geometries (the obstacle and FFS)? Another interesting questions is how will such flow dynamics like the one associated with the obstacle and FFS compare with separated-reattached boundary layers cased by a similar leading edge geometries but with no upstream separated region such as the flow dynamic associated with the square leading edge plate? To address these points, the spectra of the flow both upstream the FFS and the obstacle and that of the separated region downstream the leading edge for the three geometries will be examined first followed by flow visualisation to study the flow structure both upstream (the FFS and the obstacle) and downstream the three geometries.

4.2.1 Turbulence spectra

Extensive data for the obstacle, FFS and the square leading edge plate at different locations both the upstream (for the obstacle and FFS) and downstream separated region has been collected and processed using both the conventional Fourier transform and the wavelet spectra (not shown here). For more specific about data locations and other relevant details the reader is referred to [11] and [2].

Figures 5a and b shows the spectra for the streamwise velocity *u* and the wall-normal component *v* at a point immediately upstream of the separation line for the obstacle flow. The spectra obtained using the Fourier transform clearly show a *sharp* frequency peak (band) centered at approximately 105 Hz for both velocity components. This is equivalent to (a normalised value of) $5.425\,\frac{U_0}{x_R}$.

In almost all the work done in separated-reattached flow, the low-frequency peak in the region close to the separation line is attributed to the flapping of the shear layer. However, the normalised value for the frequency in the case of the obstacle flow ($5.425\,\frac{U_0}{x_R}$) is much higher than the corresponding value of what is termed

low-frequency motion, observed in separated-reattached flow in different geometries which is in the range of $0.1\frac{U_0}{x_R} \leq f \leq 0.18\frac{U_0}{x_R}$. Hence, it can not be attributed to the flapping of the separated boundary downstream of the leading edge of the obstacle flow. The only possible explanation for this amplified frequency is due to the K-H instabilities in the shear layer forming as a result of the small upstream separated region. In fact, the Strouhal number based on the obstacle height, the free stream velocity and the observed frequency ($St = \frac{f\,h}{U_0}$) is equivalent to $St = 0.242$. This is contained in the range $0.225 \leq St \leq 0.275$ reported by Abdalla and Yang [11] for the K-H instability. This shows further evidence that the observed frequency in the current case is due to K-H instability mechanism.

Extensive data for both the obstacle and FFS downstream the leading edge was processed and the spectra shows no trace of any amplified frequency. An example for such spectra is shown in Figures 5c and d which correspond to the streamwise velocity approximately at $\approx x/x_R = 0.5$ and the center of the shear layer for the obstacle and FFS respectively. In comparison, most of the data collected from the square leading edge plate simulation downstream the leading edge shows a peak

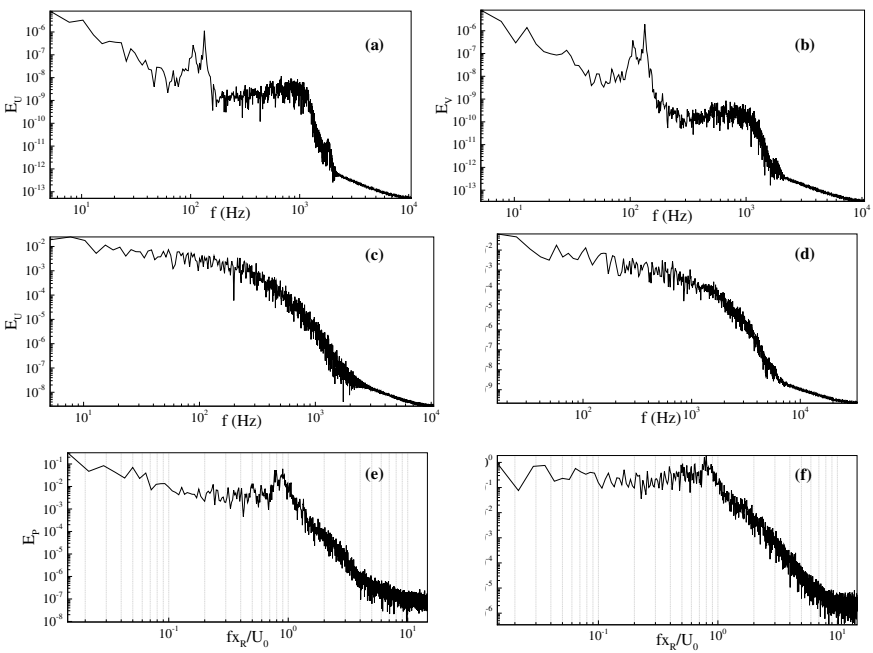

Figure 5: (a) Obstacle axial velocity at $x/h = -0.25$, $y/h = 1.05$, (b) Obstacle wall-normal velocity at $x/h = -0.25$, $y/h = 1.05$, (c) Obstacle axial velocity at $x/x_R = 0.5$, (d) FFS axial velocity at $x/x_R = 0.5$, (e) Square leading edge pressure at $x/x_R = 0.35$, (f) Square leading edge pressure at $x/x_R = 0.75$.

band of frequency, the normalised value of which is in the range $0.6 \leq \frac{f}{x_R U_0} \leq 0.8$. A sample of this is shown in figures 5e and f corresponding to the pressure spectra at $\approx x/x_R = 0.5$ and 0.75 and the center of the shear layer. The center of the shear layer is defined as the y-location where the rms value of the streamwise velocity (u_{rms}) attains a maximum value.

This fact represent the first difference between separated boundary layers on sharp leading edge geometries with an upstream separated region (such as the obstacle and FFS) and without such separated region such the square leading edge plate. It clear that the K-H instability that dominates the upstream separated region has it is influence on the spectra contents for the separated region downstream the leading edge for the obstacle and FFS. The disappearance of the shedding frequency from the spectra for the downstream separated region in the obstacle and FFS indicates that transition to turbulence may occurs much faster and that the turbulence intensity upstream the leading edge is higher when compared to the square leading edge plate flow where such frequency is quite apparent. This fact might have it is effects on the nature of instability mechanism on the downstream separated region as well as o the flow topology. However, it remains unclear how and through which mechanisms does the upstream region influence the downstream region and a separate study focusing on this point is necessary.

4.2.2 Flow structure

Figure 6 shows low-pressure isosurfaces visualising the flow topology upstream and shortly downstream the leading edge for the obstacle flow. The FFS has shown similar features and is not shown here. Figure 6 display three main features displayed associated with the flow structure upstream the obstacle and FFS. The first feature which is common to both the obstacle and FFS flows, is the existence of a quite distorted 2D structure mainly developed at $x/h = -1.0$ which exhibits a clear undulating edges. Shortly downstream the leading edge, the boundary layer rolls-up leading to the formation of 2D K-H vortices that convect downstream.

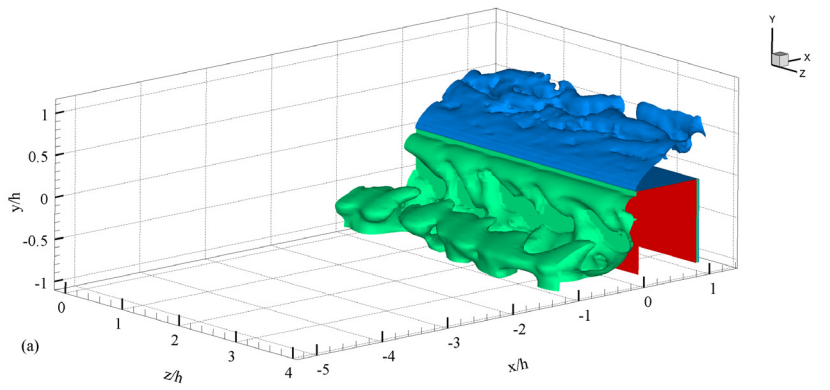

Figure 6: Flow structure of the upstream separated region of the obstacle.

The second feature displayed by the flow structure upstream of the two geometries is the existence of a 2D structure spanning the computational domain and attached to the vertical side of the obstacle/FFS immediately below the leading edge. This structure seems to be of pure 2D nature when viewed from above but when looked at from below, the structure seems very unstable and display a non-planar (wavy) edge. The reason for the waviness is what could be the third feature of the flow upstream of the obstacle/FFS flow – which is the development of vertical rib-like (streaky) structures that seems to develop from the structures itself or may be connecting it to the 3D small structures at the obstacle/FFS upstream corner. At the lower corner, there exist a smaller-scale structure which is more likely to be a result of the interaction (collision) of the 2D structure which develops at $x/h = -1$ as described above with the vertical wall. The most important part is that the structure which is attached to the vertical side of the obstacle/FFS (below the leading edge) gives the impression that there is absolutely no interaction between it and the flow downstream of the obstacle/FFS edge. In this case this means that the separation bubble upstream is a closed one and behaves in a typical way to a 2D bubble flow. However, in some occasions the 2D structure seems to get broken due to the work of the longitudinal vertical rib-like structures. This feature may indicate that parcel of fluid from the separation bubble upstream could be released into the downstream of separated region rendering the upstream bubble as an open one.

Downstream the leading of the three geometries, the flow topology is characterised by 2D K-H rolls formed as a result the boundary layer rolls-up of the laminar flow. The differences is associated with the scenarios of the evolution of such 2D coherent structures downstream the leading edge and their eventual break-up into smaller 3D structure leading to a fully turbulent flow. Figures $7a$ and b shows low-pressure isosurfacses at an arbitrary instance of time showing the flow structure downstream the obstacle and square leading edge plate, respectively. It is worth to mention that extensive data for both the obstacle and FFS was processed and all show similar features as in figure $7a$. The flow structures clearly shows that 2D K-H rolls convect downstream and eventually disintegrate into smaller turbulent structures.

Compared to the square leading edge plate flow, the picture is slightly different. As shown in Figure $7b$ the 2D K-H rolls are shed shortly down stream the leading edge and maintain their 2D nature while convicting downstream. At some stage, the continuously distorted spanwise K-H rolls are subjected to axial stretching and eventually are transformed into streamwise structures. It is reasonable to assume that the way the streamwise evolving vortices interact with the spanwise vortices is by aligning more vorticity from the spanwise into the streamwise vortices thus making them to grow and become larger while degrading the coherency of the spanwise vortical rolls. In other words the $2D$ Kelvin-Helmholtz rolls have been transformed into distinct streamwise vortical tubes. The well known Λ-shaped vortices, commonly associated with flat plate boundary layers are clearly seen in the square leading edge plate flow.

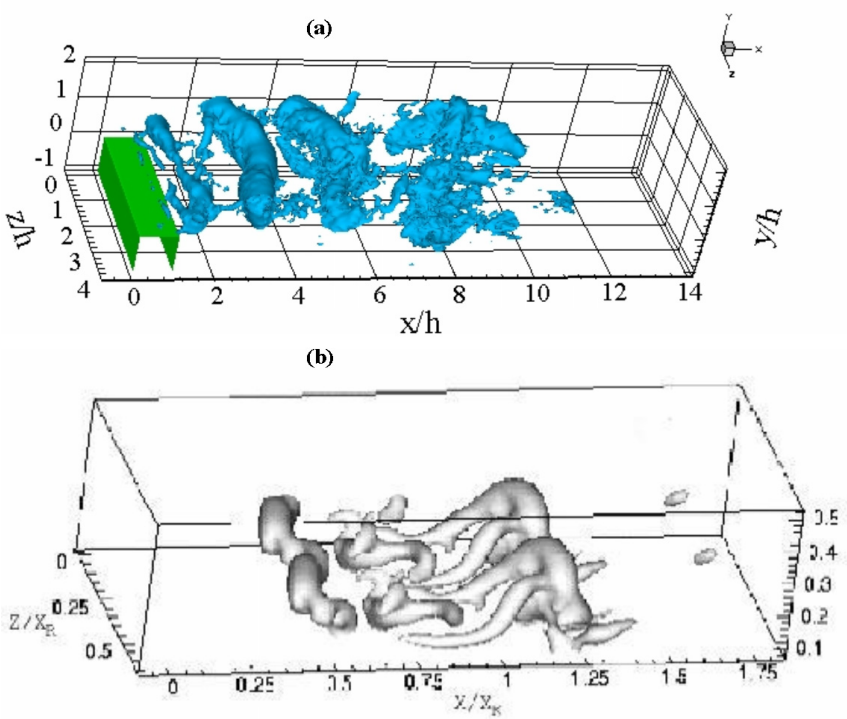

Figure 7: Flow topology downstream the leading edge: (a) the obstacle flow, (b) the square leading edge plate.

The differences in the downstream flow topology and the two distinct routes of evolution of the 2D K-H rolls strongly indicates that the nature of turbulent flow and the instability mechanisms for the two types of flows are also distinct. It is also strong indication to the fact that K-H unstable upstream separated region associated with the obstacle and FFS play some influence on the nature of the downstream turbulence characteristics and flow topology.

5 Conclusion

A comparison to some aspects of separated-reattached flows on an obstacle, FFS and a square leading edge plates indicates two fundamental differences. The characteristics shedding frequency captured in the square leading edge plate is not apparent in the obstacle and FFS flows. The flow topology downstream the obstacle and FFS leading edge has shown direct disintegrate into of the 2D K-H rolls into smaller 3D structures. For the square leading edge plate flow, 2D K-H rolls transform first into distinct 2D streamwise structures before breaking down into smaller 3D structures. It is most likely that the two differences represent an influ-

ence of the K-H unstable upstream separated region associated with the obstacle and FFS on the downstream region. A detailed quantitative analysis is required to quantify such influence.

References

[1] Yang Z., Voke, P.R. Large-eddy simulation of boundary-layer separation and transition at a change of surface curvature. *Journal of Fluid Mechanic*, **439**, 305–333, 2001.

[2] Ibrahim E. Abdalla, Malcolm J. Cook, and Zhiyin Yang. Computational analysis and flow structure of a transitional separated-reattached flow over a surface mounted obstacle and a forward-facing step. *International journal of computational fluid dynamics*, 13-1, 25–57, 2009.

[3] Bergeles, G., and Athanassiadis N.. The flow pass a surface mounted obstacle. *ASME Journal of Fluid Engineering*, **105**, 461–463, 1983.

[4] Durst, F., Rastogi, A.K. Turbulent flow over two-dimensional fences. *in Turb. Shear Flows 2*. Springer Verlag: Berlin, 218–231, 1980.

[5] Tropea, C.D., Gackstatter, R.. The flow over two-dimensional surface-mounted obstacles at low Reynolds number. *Journal of Fluids Engineering*, **107**:489–494, 1984.

[6] Orellano, A., Wengle, H.. Numerical simulation (DNS and LES) of manipulated turbulent boundary layer flow over a surface-mounted fence. *Er. J. B - Fluids*, **19**:765–788, 2000.

[7] Larsen, P.S.Database on tc-2C and tc-2D fence-on-wall and obstacle-on-wall test case. *Report AFM-ETMA 95-01, ISSN 0590-8809*; TU Denmark, 1995.

[8] Ko, S.H. Computation of turbulent flows over backward and forward-facing steps using a near-wall Reynolds stress model. *CTR Annual Research Briefs*, Stanford University/NASA Ames, 75–90, 1993.

[9] Moss, W.D., Baker, S. Re-circulating Flows Associated with Two-dimensional Steps, Aero Quart., 151–172, 1980.

[10] Castro, I.P., Epik, E. Boundary layer development after a separated region. *J. Fluid Mech*, **374**, 91–116, 1998.

[11] Abdalla, I.E., Yang, Z., 2005. Numerical study of a separated - reattached flow on a blunt plate. *AIAA Journal* **43**, 2465–2474.